Skin Research and Technology 2013; 19: e356–e365
Printed in Singapore · All rights reserved
doi: 10.1111/j.1600-0846.2012.00652.x

Skin Research and Technology

Experimental and computational analysis of soft tissue mechanical response under negative pressure in forearm

Jarkko T. Iivarinen[1,2], Rami K. Korhonen[1], Petro Julkunen[3] and Jukka S. Jurvelin[1]

[1]Department of Applied Physics, University of Eastern Finland, Kuopio, Finland,
[2]Department of Physical and Rehabilitation Medicine, Kuopio University Hospital, Kuopio, Finland and [3]Department of Clinical Neurophysiology, Kuopio University Hospital, Kuopio, Finland

Background: Instrumentation, relying on the use of negative pressure (suction), has been introduced to reduce pathological tissue swelling. Then, relative contribution of skin, adipose tissue and muscle, to the overall mechanical response is not known.

Methods: Under suction, stretch of soft tissues in the forearm of human subjects ($N = 11$) was experimentally measured at rest and under venous occlusion. Three dimensional, fibril-reinforced hyperelastic finite element (FE) model was constructed, the model response was matched with the experimental measurement and the mechanical characteristics of each tissue were derived. Parametric analyses were conducted to evaluate the impact of different tissues on the total stretch.

Results: The model suggested that, at large strains, the stretch response was more sensitive to changes in the elastic modulus of skin than those in adipose tissue. During venous occlusion, reduction of the stretch of forearm tissues was related to stiffening of the skin and adipose tissue, as evidenced by increased modulus of 27 ± 21% and 35 ± 26%, respectively.

Conclusion: The method based on suction may be used to diagnose and monitor changes in properties of soft tissues, especially those of skin, as well as tissue swelling typical to pathological conditions such as oedema.

Key words: skin – adipose tissue – muscle – collagen – suction treatment device – finite element analysis – oedema

Accepted for publication 26 April 2012

SEVERAL PATHOLOGIES, most typically soft tissue oedema, induce variations in the mechanical properties of soft tissues. Therefore, pathological development may be diagnosed by monitoring the tissue mechanical properties (1, 2). Mechanical measurements of soft tissues may rely on the use of positive or negative external stress, such as mechanical indentation or suction, respectively, and subsequent recording of tissue load and deformation. In experimental measurements, typically, different soft tissues such as skin, adipose tissue and skeletal muscle, contribute to the overall mechanical response. Unfortunately, we lack mostly the knowledge about the relative effects of different soft tissues on the measured response.

Mechanical properties of skin have been investigated using negative pressure loading in several previous studies (3–8). However, most of these studies have not taken into account the effect of underlying tissues on the measured mechanical response (3, 6). Mechanical properties of the adipose tissue (mainly fat) have been characterized by using compression tests of human breast (9–12), human heel (13, 14) or porcine tissues (15). Anisotropic mechanical properties of passive skeletal muscles have also been investigated using compression tests (16–19). In modeling studies, skin (3, 7, 8, 13), adipose tissue (20–22) and muscle (17, 23, 24) tissues are usually considered as hyperelastic. However, human skin is a heterogeneous material composed mostly of collagen and elastin fibres (3, 25). Collagenous soft tissues are often modeled as fibril-reinforced materials (26–29). There are no 3D models of human forearm to which the fibril-reinforced hyperelastic skin, and hyperelastic adipose tissue and muscle have been implemented to mimic the measured tissue stretches under negative pressure.

Instrumentation, relying on the use of negative pressure, has been introduced to stimulate

the lymph flow in order to reduce pathological tissue swelling. The instrumentation measures the degree of deformation of human soft tissues under suction. In the present study, we conducted experimental measurements to investigate soft tissue deformation of human forearm and effects of tissue swelling on the recorded mechanical response. By using a finite element (FE) model with realistic geometries of major soft tissues of human forearm (skin, adipose tissue and muscle) we simulated the experimental measurements, evaluated the effect of swelling on tissue properties, and estimated the impact of different tissues on the biomechanical response. In the model, the adipose and muscle tissue were considered to be hyperelastic material and the skin was fibril reinforced hyperelastic material. The study was established to provide answers to the specific questions, such as (1) to which degree different soft tissues control the forearm deformation under suction?; (2) how and which tissue properties change during manipulated tissue swelling? The findings of the present study can help to evaluate the diagnostic feasibility of *in vivo* suction measurements.

Materials and Methods

Study protocol

First, mechanical suction measurements were performed before and after manipulated tissue swelling in the forearm of each subject. Then, peripheral quantitative computed tomography (pQCT) images were taken to determine the dimensions of tissues at the site of mechanical measurements. The FE model geometry and mesh were based on those dimensions. The FE model was fitted to experimental measurements by optimizing the model parameters of each tissue. Finally, sensitivity of the mechanical response to changes in the mechanical properties of different tissues was evaluated by using the FE model.

Subjects and measurements

Eleven healthy volunteers (nine males, two females, age = 31 ± 7 years, height = 179 ± 9 cm, weight = 84 ± 9 kg and length of ulna bone = 29 ± 2 cm) participated in this study. Nine subjects were right-handed and two left-handed. All subjects gave their informed consent for the study. The study was approved by the Kuopio University Hospital Committee on Research Ethics (diary number 7/2010).

The treatment apparatus in use (Lympha-Touch, HLD Healthy Life Devices, Espoo, Finland) is a hand held device for treatment of post-surgical or post-traumatic oedema and lymphoedema. Using infrared light sensor, it also measures the skin rise (stretch or deformation) caused by the negative suction pressure (Fig. 1). The minor and major axes of ellipse shaped suction head are 28.0 and 43.5 mm, respectively. In treatment, the suction head, made of thermoplastic elastomer SEBS (Thermolast K, Kraiburg TPE GmbH & Co. KG, Waldkraiburg, Germany), makes a tight contact with the skin. The pressure and skin deformation were measured through the experiment with accuracies of ± 0.01 mmHg and ± 10 μm, respectively, at the sampling frequency of 40 Hz. The data was analyzed offline using Matlab (version 7.8.0, Mathworks Inc., Natick, MA, USA). Statistical analysis was performed using Wilcoxon's paired, two-sided signed rank test.

In mechanical tests, the dominant forearm of the subject was positioned to lay on a mechanical support during testing, similarly as presented earlier (30). In all the measurements, the test site was localized in the mid ulna (proximal-distal direction), centrally between the ulna and radius on the dorsal forearm. For measurements at rest (FR: forearm at rest), the test subject relaxed the forearm muscles. Subsequently, after a 5 min break, venous occlusion (VO) was created by using a pressure cuff at 8 kPa (60 mmHg) for 12 min to induce swelling of the forearm soft tissues. During each protocol, 20 repeated measurements were conducted, and the mean responses (deformation vs. suction

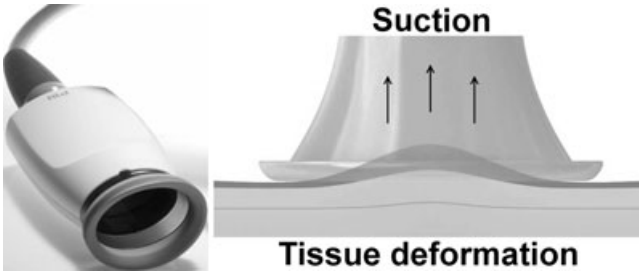

Fig. 1. Schematic presentation of treatment device used for mechanical measurements. The principle of operation, including suction and tissue stretch, is also illustrated.

pressure) of them were used as a target for model responses.

pQCT measurements

The pQCT imaging of the forearm was performed at the sites of mechanical testing (Stratec XCT 2000, Stratec Medizintechnik GmbH, Pforzheim, Germany). One image slice (thickness = 2.3 mm, pixel size = 0.2 mm × 0.2 mm) was taken from each subject [Fig. 2(a)]. Different tissue layers were manually segmented from the images, and the tissue areas were calculated using Matlab. The location of tissue midpoint was also based on pQCT measurements.

FE model and simulations

Using the pQCT images the model geometry was constructed by first simplifying each tissue cross-section to be of circular shape [Fig. 2(b)]. Then, a circular shaped cross-section area, defined by the circle radius, of each tissue in the model was matched with the measured cross-section area (Table 1). Finally, the 2D geometry was extruded to 3D, achieving a cylindrical shape for the model geometry [Fig. 2(c)].

Three different models were created; one was based on the mean experimental results of all subjects ($N = 11$), while two were based on measurement results of two individuals with clearly different (maximum, minimum) tissue responses. The FE model (Fig. 3) was created and simulations were conducted using ABAQUS 6.9 (SIMULIA, Dassault Systèmes, Providence, RI, USA). In the model geometry, the forearm was 30 cm in length, long enough to exclude any edge effects. The suction head consisted of 3063–6774 rigid 4-node surface elements (R3D4) and the tissues of 24860–32976 hexahedral 8-node elements with reduced integration points (C3D8R). The mesh at the areas of interest (in close proximity of the suction area) was made denser to obtain smoother stress/strain distributions. Optimal density for the FE mesh was found after running a convergence study. Contact between the suction head and the skin was assumed to be frictionless. The ulna and radius bones in the model were considered to be rigid and static by restricting the movement of the muscle nodes in contact with the bones. As the perimeter of the bones was fixed to be stationary, there was no need to use elements inside the bones. The movement of the nodes at the edge of the muscle was restricted. The suction pressure field was modeled to be shaped as a portion of a sphere (5), exposed on the skin surface within the suction area.

Muscle and adipose tissue were modeled as Neo-Hookean hyperelastic material. The Neo-Hookean material can imitate closely the mechanical behaviour of biological soft tissues, especially skin and adipose tissue, under short-term loading (9, 30–35). As the Neo-Hookean material is defined with only two parameters, optimization of the material parameters is straightforward. The strain energy potential function of the Neo-Hookean model is expressed in the form

TABLE 1. Radius of different tissue layers (circular approximation) used in the finite element models. Mean of the group (N = 11) and separately for subjects 1 (s_1) and 2 (s_2).

	Tissue layer radius (mm)				
Subject(s)	Skin	Adipose tissue	Muscle	Radius (bone)	Ulna
Group ($N = 11$)	40.9	39.3	36.2	6.8	7.1
s_1	38.9	37.2	34.7	7.0	7.3
s_2	40.0	38.3	34.8	7.0	7.2

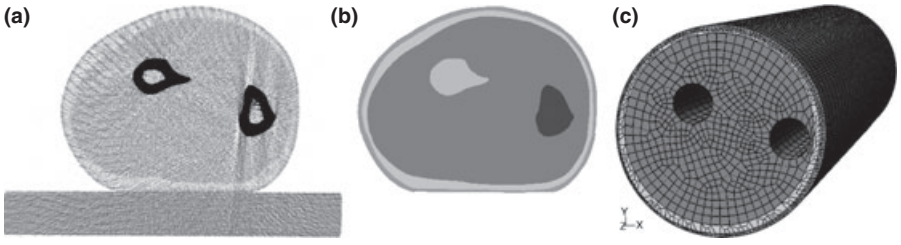

Fig. 2. (a) pQCT image of the forearm of a single subject. The image was used to measure areas of different tissues. Pixel size was 0.2 mm × 0.2 mm. (b) Image after tissue segmentations with arm support removed and (c) the simplified geometry used for FE simulations.

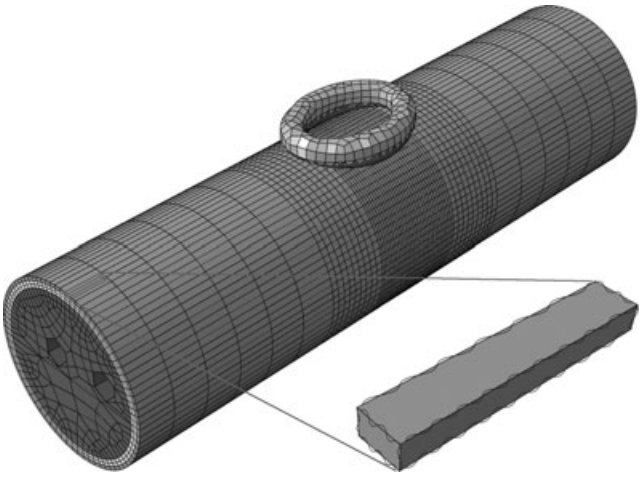

Fig. 3. Geometry and mesh of the FE model. Different tissue areas are indicated with different colours. The fibres are visualized as springs within the magnified element. The suction head consisted of 3063 and the tissues of 26137 elements.

$$U = C_{10}(\bar{I}_1 - 3) + \frac{1}{D_1}(J^{el} - 1)^2 \quad (1)$$

, where $\bar{I}_1$ is the first deviatoric strain invariant, J^{el} the elastic volume ratio and C_{10} and D_1 are parameters defining the shear behaviour

$$C_{10} = \frac{G_0}{2} = \frac{E}{4(1+v)} \quad (2)$$

and the bulk behaviour

$$D_1 = \frac{2}{B_0} = \frac{6(1-2v)}{E} \quad (3)$$

In Eqs (2) and (3), G_0 is the initial shear modulus, B_0 the initial bulk modulus, E the elastic modulus and v the Poisson's ratio. Therefore, both C_{10} and D_1 can be expressed with E and v. The Poisson's ratio for each tissue was fixed to 0.4, similarly to previous studies (2, 17, 19, 30, 36, 37).

Hyperelastic material was not considered to describe skin behavior realistically (3), as revealed by our preliminary and validation simulations. Therefore, fibril-reinforcement was added to the skin properties. This was realized by using nonlinear springs (SPRINGA element type in Abaqus), which were aligned lengthwise along tension axis. Properties of the collagen fibers could then be described by the fibril network modulus $E_f = \Delta\sigma/\Delta\varepsilon$ [Fig. 4(a)]. We also added ε_0, the toe limit strain, in the model to describe the possible effect of fibril straightening; larger ε_0 indicates longer tissue elongation before collagen fibers have been straightened. The initial properties of the fibril-reinforced hyperelastic (FRHE) model were obtained by capturing the mechanical tensional response of skin presented experimentally in (38). The FRHE material was, while simple neo-Hookean hyperelastic (HE) material was not, able to capture the mechanical response [Fig. 4(b)]. In these simulations, the optimized properties of the FRHE skin were: E_{skin} = 115 MPa, ε_0 = 3.6% and E_f = 0.43 GPa. The mean absolute error between the experimental measurements and simulations was less than 0.3%.

As the mechanical role of the muscles was found minimal in the model, the elastic modulus of the muscle was fixed to 100 kPa (17, 30, 36, 39, 40). The fibril network modulus values of over 50 MPa produced similar tissue stretches (see below, Fig. 9), thus, it was fixed to a literature value of 4.4 GPa (41). Optimization of the material properties was conducted for the elastic modulus of skin, toe limit strain of skin fibrils and elastic modulus of adipose tissue by minimizing the mean squared error (MSE) between the simulated and experimental responses using a multidimensional unconstrained nonlinear minimization routine, utilizing Nelder-Mead method available in Matlab.

Sensitivity of the tissue stretch in the forearm to the mechanical parameters of different tissues was investigated. In the FE model the values of the elastic modulus for skin, adipose tissue and muscle were altered independently from 50% to 200% of the optimized reference values, and the effects on the mechanical response were analyzed. Similarly, significance of the fibril network modulus and the toe limit strain of skin was analyzed.

Results

After the VO, the skin deformation was reduced by 7.9 ± 9.5% (N = 11, Fig. 5). The measured differences in responses during FR and VO were statistically significant ($P < 0.05$). Values of the elastic modulus of skin and adipose tissue, as obtained by fitting the model to the experimental data at rest, were 1.13 ± 0.21 MPa and 0.80 ± 0.36 kPa (mean ± SD), respectively (Fig. 6, Table 2). The fibril toe limit strain at rest was 2.8 ± 1.4%. As a result of the VO, the

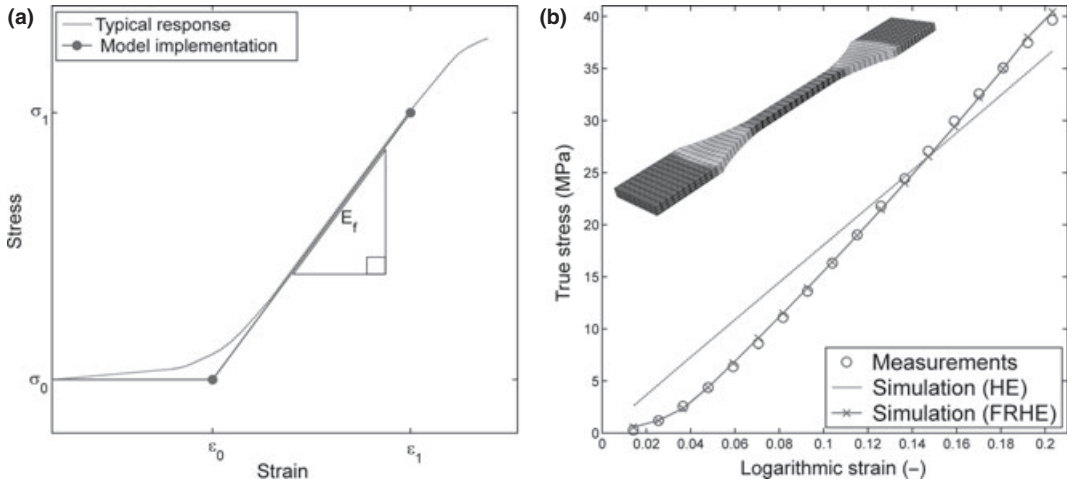

Fig. 4. (a) Typical mechanical response of collagenous skin in tension (red curve) with the implemented response in the present skin model (blue curve). (b) Geometry for a tension measurement with the experimental response (38) to test the suitability of the hyperelastic (HE) and the fibril-reinforced hyperelastic (FRHE) skin models. The mean absolute error between the experimental measurements and the FRHE model was less than 0.3%.

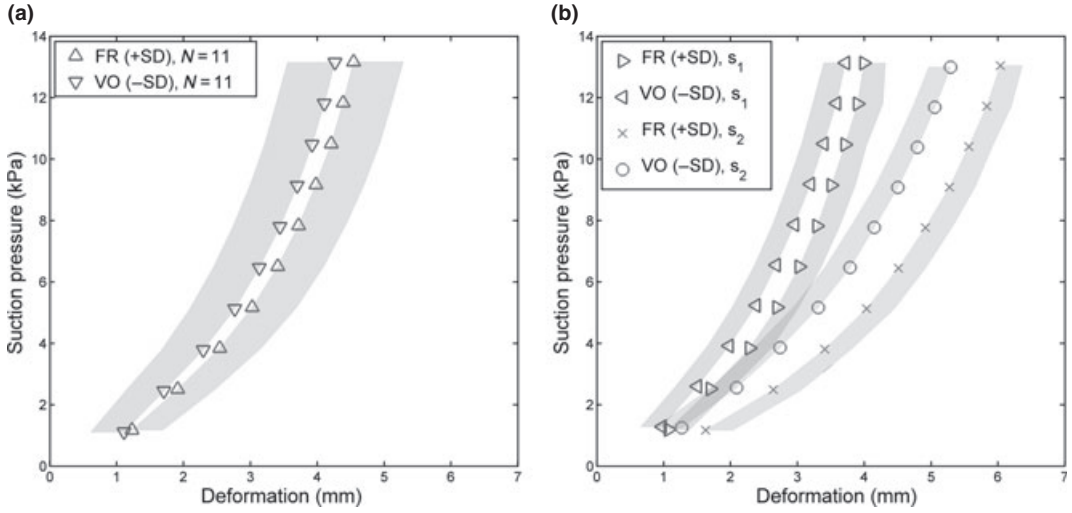

Fig. 5. Experimental results (Mean ± SD) at rest (FR) and under venous occlusion (VO). (a) the mean response, (b) the response of subjects 1 (s_1) and 2 (s_2). Difference between the measured responses during FR and VO was statistically significant ($P < 0.05$).

optimized modulus values of the skin and adipose tissue increased by 27 ± 21% and 35 ± 26%, respectively. The difference between the experimental and the FE data was less than 1.0% in all loading configurations.

The highest von Mises stress values were located in the skin layer, at the longitudinal edges of the instrument suction head (Fig. 7). The highest logarithmic strain values were present in the adipose tissue layer, and located under the center of the suction head. The maximum von Mises stress value under the FR/VO condition was 61.2 ± 8.9/64.1 ± 13.7 kPa for the skin, 1.0 ± 0.2/0.9 ± 0.2 kPa for the adipose tissue and 1.6 ± 0.6/2.0 ± 0.6 kPa for the muscle. The maximum logarithmic strain value under the FR/VO condition was 0.04 ± 0.01/0.04 ± 0.00 for the skin, 0.94 ± 0.07/0.87 ± 0.05 for the adipose tissue and 0.02 ± 0.01/0.02 ± 0.01 for the muscle.

Based on the parametric analyses, sensitivity of the deformation registered by the instrument to different tissue properties varied along the level of tissue deformation. Under small deformation (<2 mm), the model response was slightly more (up to 13%) sensitive to changes in the elastic modulus of the adipose tissue than to those of the skin. Under large deformation

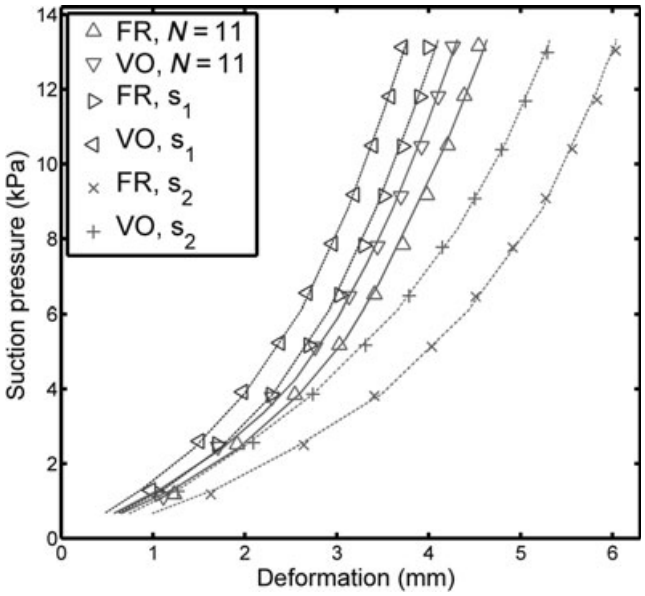

Fig. 6. Experimental and model responses at rest (FR) and under venous occlusion (VO). Mean response (N = 11) and that of subjects 1 (s_1) and 2 (s_2).

TABLE 2. Optimized values (mean value of the group and subjects 1 (s_1) and 2 (s_2) separately) for elastic modulus of skin, E_{skin}, and adipose tissue, $E_{a.t.}$, and the fibril toe limit strain ε_0. The fibril network modulus, E_f, was constant (4.4 GPa) in all models. FR – forearm at rest, VO – venous occlusion.

Subject(s)	Measurement condition	E_{skin} (kPa)	$E_{a.t.}$ (kPa)	ε_0 (%)
Group	FR	948	1.17	2.08
(N = 11)	VO	1151	1.30	
s_1	FR	1364	0.77	1.86
	VO	1500	1.26	
s_2	FR	1071	0.45	4.40
	VO	1613	0.59	

(>3 mm), the model response was substantially more (up to 86%) sensitive to changes in the elastic modulus of the skin than to those of the adipose tissue (Fig. 8). Further, under large deformation, the modeled response was up to 54% more sensitive to changes in the fibril toe limit strain than in the elastic modulus of the adipose tissue. The modulus of muscle and the fibril network modulus of skin (when > 50 MPa) had only minor effects on the model response (Figs 8 and 9).

Discussion

Pathological tissue swelling, a characteristic condition related to post-surgical or post-traumatic oedema and lymphoedema, is characterized by impaired lymph flow. Therapeutic instrumentation (LymphaTouch, HLD Healthy Life Devices, Espoo, Finland), applying a negative pressure, *i.e.* suction, has been introduced to stimulate the lymph flow. The treatment instrumentation has been designed to simultaneously measure deformation of human soft tissues, sensitively altered by pathological tissue swelling. Ideally, the mechanical measurement could provide direct information on the effect of treatment protocol. However, under negative pressure, the relative contribution of each soft tissue component, *i.e.* skin, adipose tissue and muscle, to the overall measured mechanical response is not known. In the present study, mechanical responses of human forearm soft tissues were measured at rest and under venous occlusion using a LymphaTouch device. A FRHE model with the geometry obtained from pQCT imaging was created to determine the elastic modulus of skin and adipose tissue, as well as deformational behavior of the skin fibrils, in the forearm. We specifically found that: (1) the suction device in use observes sensitively the mechanical properties of the skin, especially under large tissue deformation, (2) during manipulated tissue swelling, the skin and the adipose tissue stiffen simultaneously.

The present values for the skin elastic modulus (948–1364 kPa) are consistent with those reported earlier. In fact, the reported values show high variation, from 8 kPa up to 540 MPa (3–5, 30, 42). Also, the values of elastic modulus for the adipose tissue (0.45–1.17 kPa) agree with those reported in earlier studies, i.e., 0.5–5.6 kPa (36, 43, 44). Similar parameter, as the fibril toe limit strain in the present study, has been introduced for skin (3) and for human spine or rat tendon collagen using *in vitro* measurements (45, 46). This parameter is strongly affected by the initial stress/strain level of the skin, consistent with earlier studies. The present experimental method, combined with the computational analysis, was found to characterize skin and adipose tissue properties realistically.

According to parametric analyses, the modeled deformation was most sensitive to changes in the elastic modulus of the skin, although degree of tissue deformation significantly affected the sensitivity (Fig. 8). Under small deformation, the model response was sensitive to changes in the elastic modulus of the adipose tissue while, under large deformation, the response of the model was strongly affected by

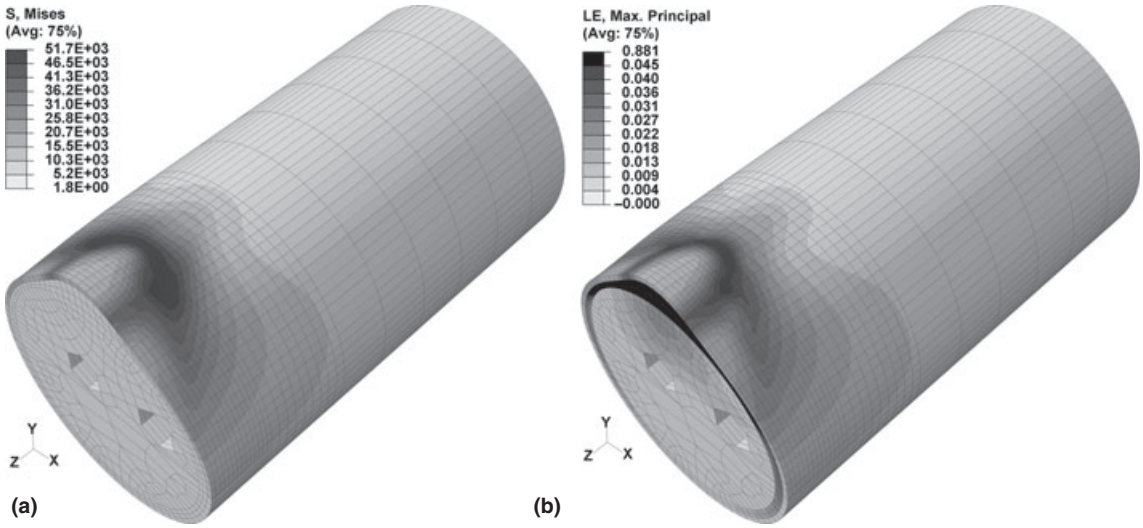

Fig. 7. (a) von Mises stress (S) and (b) logarithmic strain (LE) distributions in the forearm tissues at rest under 13.3 kPa suction pressure. The highest von Mises stress value (51.9 kPa) was located in the skin at the longitudinal ends of the stretched area. The highest logarithmic strain value (0.88) was located in the adipose tissue under the suction area of the skin.

the changes in the elastic modulus of the skin and fibril toe limit strain. The effect of the muscle stiffness on the modeled suction response was minor. These results clearly highlight the importance of skin properties on the results obtained by using the present therapy instrument.

Variations (50%–200% of the reference value) in the values of the fibril network modulus had negligible effects on the model response. Only values lower than 50 MPa increased the error between the model and experiment (Fig. 9). This finding was related to rapid stiffening of the collagen after the fibril toe limit strain was exceeded. In fact, collagen has tensile strength comparable to steel (47) and the fibrils might swiftly turn nearly unstretchable (considering the forces present in the model).

The cuff pressure in use (60 mmHg) was considered to provide sufficient external pressure to keep the superficial veins occluded (48). The short-term venous occlusion prevents the veins from transporting the blood towards heart and causes the veins to swell, observed in this study mostly by local stiffening of skin and adipose tissue.

In the present study, friction between the skin and the suction head could not be measured. Therefore, this interface was assumed frictionless. Using the FE model, variations in the friction coefficient between 0.3 and 0.9 altered the mean skin deformation by 2.7%–6.7%, suggesting that the friction effects may not be negligible in the experimental suction measurements. When the suction head was modeled to be elastic (E = 2.83 MPa, v = 0.49), instead of rigid material, 0.7% variation in the modeled response was demonstrated. This suggests that the assumption of a rigid suction head is an acceptable simplification.

There are limitations and simplifications in the material description of our FE model. Skin fibres were aligned parallel to the skin surface, making skin anisotropic. Due to simplicity required by the optimization process we could not differentiate between longitudinal and transversal fibres. The mechanical response of the collagenous fibril network in skin is usually considered to consist of three phases: low stiffness phase (crimped fibres), toe region (straightening of fibres) and elastic linear phase (straight fibres). This response was simplified by two phases [Fig. 4(a)] to minimize the number of parameters for optimization. The simplification was considered acceptable, as also suggested by the small error between the experimental test and the model prediction.

The realistic soft tissue geometry in the forearm is complex, and the amount and shape of each tissue alters from wrist to elbow. Fully realistic tissue geometry, reproduced from pQCT images, created many areas with distorted elements in the model. Therefore, in the present study, the 3D geometry of each tissue was simplified and modeled to be of cylindrical shape. This simplification may slightly change

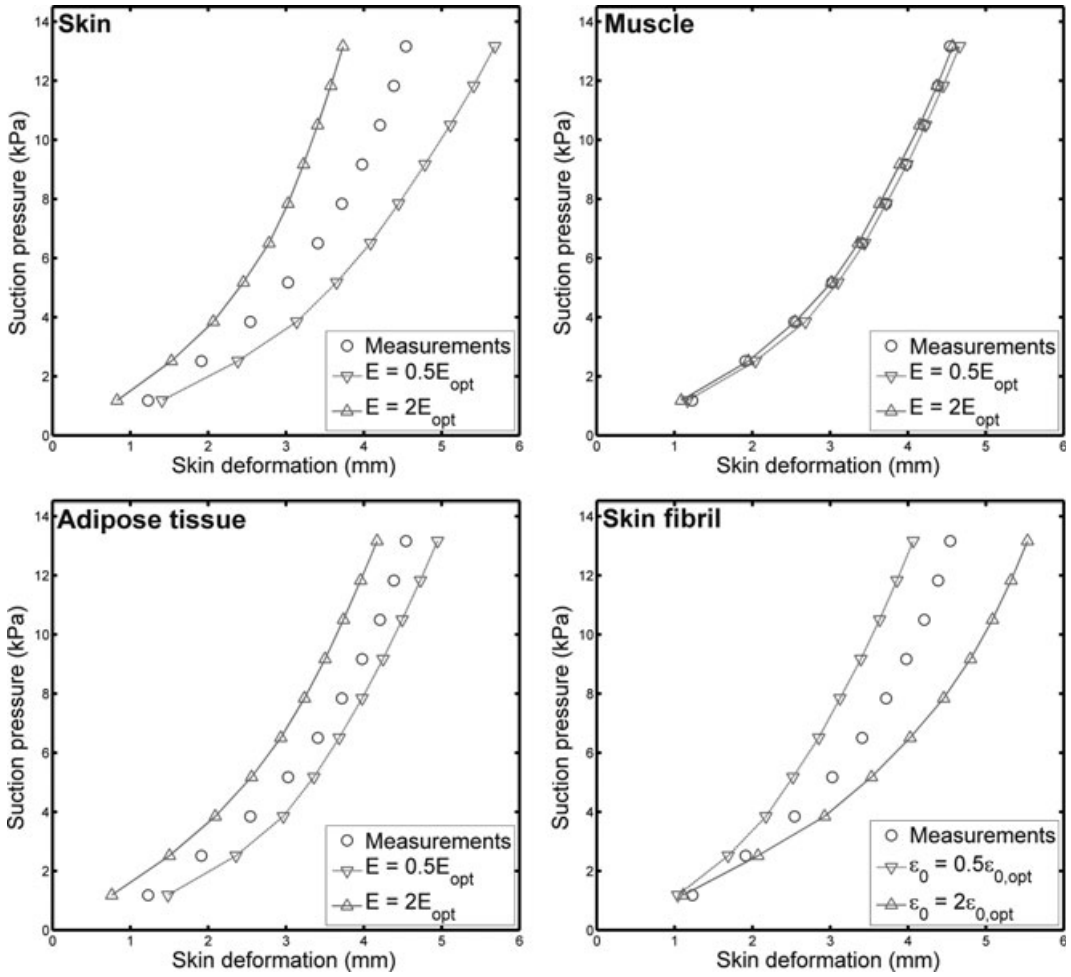

Fig. 8. Parametric analysis. Simulated deformation with different values of elastic modulus E for each tissue (skin, adipose tissue, muscle) and fibril toe limit strain ε_0. The tissue parameters were changed independently from 50% to 200% of the reference value.

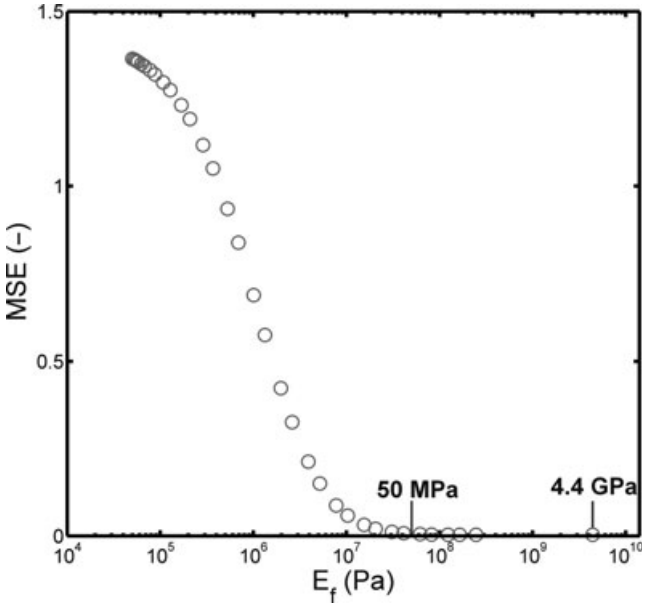

Fig. 9. Effect of the value of fibril network modulus E_f on the mean squared error (MSE), calculated by comparing the experimental and model responses.

the absolute values of the material parameters obtained from the optimization, but it should not influence the main conclusions of the study.

The present method could be applied to other body parts as well. The fluid-dependent viscoelasticity of the tissues could be incorporated in the model, especially if the time-dependent responses are analyzed. Fluid flow during short-term suction is minor or negligible, however, a more versatile model would be useful for investigating the time-dependent responses.

In conclusion, FE modeling provides a feasible method to evaluate factors affecting suction responses of inhomogeneous soft tissues. The present model was able to address the role and significance of different tissues (skin, adipose tissue, muscle) on the suction responses recorded by the experimental device. Based on the present results, the *in vivo* measurements with the device can be used to monitor changes in the mechanical properties of soft tissues,

especially those of the skin and adipose tissue. Therefore, the suction device can be useful when diagnosing and monitoring changes in soft tissue properties and tissue swelling, typical to pathological conditions such as oedema.

Acknowledgement

This study was funded by the Finnish Funding Agency for Technology and Innovation (TEKES), Northern Savo Hospital District (EVO – special state subsidy) and the Academy of Finland (grant 218038). Further, the strategic funding of the University of Eastern Finland was used. CSC – IT Center for Science, Finland, is acknowledged for computational resources and technical support.

Conflict of interest statement

Authors have no conflicts of interest.

References

1. Han L, Noble JA, Burcher M. A novel ultrasound indentation system for measuring biomechanical properties of in vivo soft tissue. Ultrasound Med Biol 2003; 29: 813–823.
2. Diridollou S, Pavy-Le Traon A, Maillet A et al. Characterisation of gravity-induced facial skin oedema using biophysical measurement techniques. Skin Res Technol 2000; 6: 118–127.
3. Delalleau A, Josse G, Lagarde JM, Zahouani H, Bergheau JM. A nonlinear elastic behavior to identify the mechanical parameters of human skin in vivo. Skin Res Technol 2008; 14: 152–164.
4. Diridollou S, Black D, Lagarde JM et al. Sex- and site-dependent variations in the thickness and mechanical properties of human skin in vivo. Int J Cosmet Sci 2000; 22: 421–435.
5. Diridollou S, Patat F, Gens F et al. In vivo model of the mechanical properties of the human skin under suction. Skin Res Technol 2000; 6: 214–221.
6. Hendriks FM, Brokken D, Oomens CW, Baaijens FP. Influence of hydration and experimental length scale on the mechanical response of human skin in vivo, using optical coherence tomography. Skin Res Technol 2004; 10: 231–241.
7. Hendriks FM, Brokken D, Oomens CW, Bader DL, Baaijens FP. The relative contributions of different skin layers to the mechanical behavior of human skin in vivo using suction experiments. Med Eng Phys 2006; 28: 259–266.
8. Hendriks FM, Brokken D, van Eemeren JT, Oomens CW, Baaijens FP, Horsten JB. A numerical-experimental method to characterize the non-linear mechanical behaviour of human skin. Skin Res Technol 2003; 9: 274–283.
9. Chung JH, Rajagopal V, Nielsen PM, Nash MP. A biomechanical model of mammographic compressions. Biomech Model Mechanobiol 2008; 7: 43–52.
10. Samani A, Bishop J, Yaffe MJ, Plewes DB. Biomechanical 3-D finite element modeling of the human breast using MRI data. IEEE Trans Med Imaging 2001; 20: 271–279.
11. Samani A, Plewes D. A method to measure the hyperelastic parameters of ex vivo breast tissue samples. Phys Med Biol 2004; 49: 4395–4405.
12. Wang ZG, Liu Y, Wang G, Sun LZ. Elastography method for reconstruction of nonlinear breast tissue properties. Int J Biomed Imaging 2009; 2009: 406854.
13. Flynn C, McCormack BA. Finite element modelling of forearm skin wrinkling. Skin Res Technol 2008; 14: 261–269.
14. Miller-Young JE, Duncan NA, Baroud G. Material properties of the human calcaneal fat pad in compression: experiment and theory. J Biomech 2002; 35: 1523–1531.
15. Wu JZ, Cutlip RG, Andrew ME, Dong RG. Simultaneous determination of the nonlinear-elastic properties of skin and subcutaneous tissue in unconfined compression tests. Skin Res Technol 2007; 13: 34–42.
16. Aritan S, Oyadiji SO, Bartlett RM. A mechanical model representation of the in vivo creep behaviour of muscular bulk tissue. J Biomech 2008; 41: 2760–2765.
17. Linder-Ganz E, Gefen A. Mechanical compression-induced pressure sores in rat hindlimb: muscle stiffness, histology, and computational models. J Appl Physiol 2004; 96: 2034–2049.
18. Van Loocke M, Lyons CG, Simms CK. Viscoelastic properties of passive skeletal muscle in compression: stress-relaxation behaviour and constitutive modelling. J Biomech 2008; 41: 1555–1566.
19. Van Loocke M, Lyons CG, Simms CK. A validated model of passive muscle in compression. J Biomech 2006; 39: 2999–3009.
20. Wu JZ, Dong RG, Schopper AW. Analysis of effects of friction on the deformation behavior of soft tissues in unconfined compression tests. J Biomech 2004; 37: 147–155.
21. Wu JZ, Dong RG, Smutz WP, Schopper AW. Modeling of time-dependent force response of fingertip to dynamic loading. J Biomech 2003; 36: 383–392.
22. Wu JZ, Welcome DE, Dong RG. Three-dimensional finite element simulations of the mechanical response of the fingertip to static and dynamic compressions. Comput Methods Biomech Biomed Eng 2006; 9: 55–63.
23. Cox SL, Mithraratne K, Smith NP. An anatomically based finite element model of the lower limbs in the seated posture. Conf Proc IEEE Eng Med Biol Soc 2007; 2007: 6327–6330.
24. Jia Z, Du Z, Monan W. A novel finite element method based biomechanical model for HIT-robot assisted orthopedic surgery system. Conf Proc IEEE Eng Med Biol Soc 2006; 1: 1735–1738.
25. Bischoff JE, Arruda EM, Grosh K. Finite element modeling of human skin using an isotropic, nonlinear elastic constitutive model. J Biomech 2000; 33: 645–652.
26. Julkunen P, Kiviranta P, Wilson W, Jurvelin JS, Korhonen RK. Characterization of articular cartilage by combining microscopic analysis with a fibril-reinforced finite-element model. J Biomech 2007; 40: 1862–1870.
27. Li LP, Cheung JT, Herzog W. Three-dimensional fibril-reinforced

finite element model of articular cartilage. Med Biol Eng Comput 2009; 47: 607–615.
28. Goh KL, Meakin JR, Aspden RM, Hukins DW. Stress transfer in collagen fibrils reinforcing connective tissues: effects of collagen fibril slenderness and relative stiffness. J Theor Biol 2007; 245: 305–311.
29. Mononen ME, Mikkola MT, Julkunen P et al. Effect of superficial collagen patterns and fibrillation of femoral articular cartilage on knee joint mechanics-A 3D finite element analysis. J Biomech 2011; 45: 579–587.
30. Iivarinen JT, Korhonen RK, Julkunen P, Jurvelin JS. Experimental and computational analysis of soft tissue stiffness in forearm using a manual indentation device. Med Eng Phys 2011; 33: 1245–1253.
31. Portnoy S, Yizhar Z, Shabshin N et al. Internal mechanical conditions in the soft tissues of a residual limb of a trans-tibial amputee. J Biomech 2008; 41: 1897–1909.
32. del Palomar AP, Calvo B, Herrero J, Lopez J, Doblare M. A finite element model to accurately predict real deformations of the breast. Med Eng Phys 2008; 30: 1089–1097.
33. Sims AM, Stait-Gardner T, Fong L et al. Elastic and viscoelastic properties of porcine subdermal fat using MRI and inverse FEA. Biomech Model Mechanobiol 2010; 9: 703–711.
34. Tran HV, Charleux F, Rachik M, Ehrlacher A, Ho Ba Tho MC. In vivo characterization of the mechanical properties of human skin derived from MRI and indentation techniques. Comput Methods Biomech Biomed Eng 2007; 10: 401–407.
35. Geerligs M, van Breemen L, Peters G, Ackermans P, Baaijens F, Oomens C. In vitro indentation to determine the mechanical properties of epidermis. J Biomech 2011; 44: 1176–1181.
36. Ohl SW, Klaseboer E, Khoo BC. The dynamics of a non-equilibrium bubble near bio-materials. Phys Med Biol 2009; 54: 6313–6336.
37. Wu JZ, Dong RG, Smutz WP, Schopper AW. Nonlinear and viscoelastic characteristics of skin under compression: experiment and analysis. Biomed Mater Eng 2003; 13: 373–385.
38. Kang G, Wu X. Ratchetting of porcine skin under uniaxial cyclic loading. J Mech Behav Biomed Mater 2011; 4: 498–506.
39. Levinson SF, Shinagawa M, Sato T. Sonoelastic determination of human skeletal muscle elasticity. J Biomech 1995; 28: 1145–1154.
40. Zil'bergleit AS, Zlatina IN, Siniakov VS, Khaikova MI. Method of measuring the modulus of elasticity of human muscle tissue. Biull Eksp Biol Med 1983; 96: 101–105.
41. Fratzl P. Collagen: structure and mechanics. New York: Springer, 2008.
42. Khatyr F, Imberdis C, Vescovo P, Varchon D, Lagarde JM. Model of the viscoelastic behaviour of skin in vivo and study of anisotropy. Skin Res Technol 2004; 10: 96–103.
43. Rajagopal V, Lee A, Chung JH et al. Towards tracking breast cancer across medical images using subject-specific biomechanical models. Med Image Comput Comput Assist Interv 2007; 10(Pt 1): 651–658.
44. Samani A, Zubovits J, Plewes D. Elastic moduli of normal and pathological human breast tissues: an inversion-technique-based investigation of 169 samples. Phys Med Biol 2007; 52: 1565–1576.
45. Shah JS, Jayson MI, Hampson WG. Low tension studies of collagen fibres from ligaments of the human spine. Ann Rheum Dis 1977; 36: 139–145.
46. Young RG, Butler DL, Weber W, Caplan AI, Gordon SL, Fink DJ. Use of mesenchymal stem cells in a collagen matrix for achilles tendon repair. J Orthop Res 1998; 16: 406–413.
47. Doering CW, Jalil JE, Janicki JS et al. Collagen network remodelling and diastolic stiffness of the rat left ventricle with pressure overload hypertrophy. Cardiovasc Res 1988; 22: 686–695.
48. Kolari PJ. A model approach for calculating the net capillary filtration rate during venous occlusion. Clin Physiol 1993; 13: 11–17.

Address:
Jarkko T. Iivarinen
Department of Applied Physics
University of Eastern Finland
Yliopistonranta 1F
70211 Kuopio
Finland
Tel: +358407007121
Fax: +35817162585
e-mail: jarkko.iivarinen@uef.fi